THE JOURNAL OF PHYSICAL CHEMISTRY C
A JOURNAL OF THE AMERICAN CHEMICAL SOCIETY

pubs.acs.org/JPCC

Article

Metal Exchange Boosts the CO_2 Selectivity of Metal Organic Frameworks Having Zn-Oxide Nodes

Gokay Avci, Cigdem Altintas, and Seda Keskin*

Cite This: *J. Phys. Chem. C* 2021, 125, 17311−17322

Read Online

ACCESS | Metrics & More | Article Recommendations | Supporting Information

ABSTRACT: A large number of metal organic frameworks (MOFs) synthesized to date have nodes with a Zn metal, and a detailed understanding of their gas separation efficiency upon metal exchange is needed to pave the way for designing the next generation of MOFs. In this work, we implemented a protocol to identify MOFs with Zn nodes out of 10,221 MOFs and classified them into two main groups. Depending on the pore properties and adsorption selectivities, two MOFs from IRMOFs and two MOFs from ZnO-MOFs were selected. The metal atom (Zn) of the selected four MOFs was exchanged with eight different metals (Cd, Co, Cr, Cu, Mn, Ni, Ti, and V), and 32 different metal-exchanged MOFs (M-MOFs) were obtained. By performing grand canonical Monte Carlo simulations, we investigated the influence of the metal type on the CO_2/H_2 and CO_2/CH_4 separation performances of these 32 M-MOFs. Physical properties of the MOFs such as the pore size and surface area, and chemical properties such as the partial charges of the atoms in the framework were investigated to understand the effect of metal exchange on the gas adsorption and separation performances of materials. Exchange of Zn with V and Cr led to a remarkable increase in the CO_2 uptakes of selected MOFs and these increases were reflected on the adsorption selectivity, working capacity, and the adsorbent performance score of MOFs. The exchange of Zn with V increased the selectivity of one of the MOFs from 119 to 355 and the adsorbent performance score from 70 to 444 mol/kg, while for another MOF, exchange of Zn with Cr increased the selectivity from 161 to 921 and the adsorbent performance score from 162 to 1233 mol/kg under the condition of vacuum swing adsorption. The molecular level insights we provided to explain the improvement in the gas separation performances of M-MOFs will serve as a guide to design materials with exceptional CO_2 separation performances.

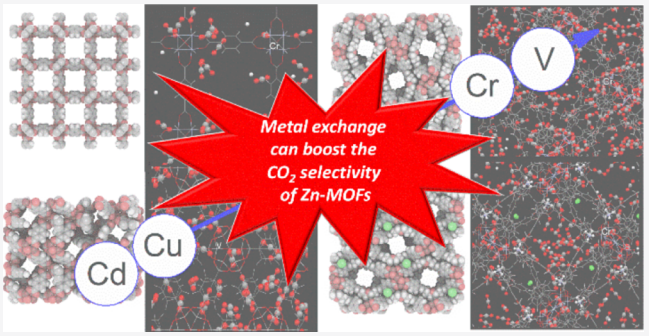

1. INTRODUCTION

Metal organic frameworks (MOFs) are promising adsorbents with high CO_2 capture capacity due to their unique crystal structures and great degree of tunability.[1,2] MOFs can be easily modified to achieve high porosities,[3] record surface areas,[4] and a wide range of pore sizes and shapes.[5] Several experimental and computational studies have shown that MOFs outperform many traditional zeolites in CO_2 capture from the CO_2/H_2 mixture.[3,6,7] To further harness the tremendous potential of MOFs, a recent direction has been changing the metal type in the structure to generate a new MOF. The strong influence of the metal choice on the CO_2 uptake has long been known in the field especially with the MOF-74 series,[8] as the CO_2 uptake of a Zn-DOBDC analog, Mg-DOBDC, was experimentally measured as 23.6 wt % at 0.1 bar, 296 K, almost four times higher than that of Zn-DOBDC and two times higher than those of Ni- and Co-DOBDC. Therefore, changing the metal type in a structure to develop a new MOF with an improved gas uptake is quite a useful approach to further harness the immense potential of MOFs. Various experimental techniques have been employed for metal substitution such as direct synthesis,[9] postsynthetic metal exchange,[10] and cluster metal-ation through stepwise synthesis,[11] which allowed the investigation of metal-exchanged MOFs, M-MOFs, where M corresponds to the metal identity. Metal exchange techniques have been widely applied on commonly studied MOFs such as HKUST-1,[12] IRMOF-10,[13] and UiO-66,[14] and the impact of metal exchange on the adsorption of gases such as CO_2, CH_4, N_2, and H_2 was investigated. In direct synthesis methods, it is not possible to foresee whether the new M-MOF will retain the original crystal structure and maintain its permanent porosity,[15] and in the postsynthetic metal exchange method, partial metal exchange may hinder the gas adsorption potential of MOFs.[16] Therefore, it is not experimentally viable to exercise all possible metal combinations in a MOF using a trial-and-error approach. Computational studies are very useful to

Received: April 22, 2021
Revised: July 9, 2021
Published: July 30, 2021

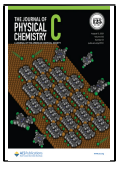

https://doi.org/10.1021/acs.jpcc.1c03630
J. Phys. Chem. C 2021, 125, 17311−17322

alter the type of metal in a MOF, which allows in silico discovery of new MOFs with exceptional CO_2 adsorption and separation performances.

Cu−Cu paddlewheel MOFs are one of the most commonly examined M-MOFs in the literature.[17] H_2 uptake of M-BTC, where M = Co, Ni, Fe, and Zn, was experimentally compared with that of Cu-BTC and gravimetric uptakes were found to increase by 10, 58, 59, and 60% for Co, Ni, Fe, and Zn-BTC, respectively.[18] By postsynthetic partial metal substitution, O_2/N_2 selectivities of Mn-, Fe-, and Co-exchanged Cu-BTC were experimentally found to be higher than the O_2/N_2 selectivity of Cu-BTC in the order of Mn-BTC > Fe-BTC ≈ Co-BTC ≫ Cu-BTC at 77 K, which was supported with the difference in binding energies for O_2 and N_2 in M-MOFs calculated with density functional theory.[19] However the metal centers were not attractive as at cryogenic temperatures (77 K) for O_2 and N_2 molecules at ambient temperatures (273, 283, and 298 K). Isoreticular MOFs (IRMOFs) have been widely studied due to their high chemical stabilities and wide range of surface areas (500 to 5500 m^2/g).[20] Partial Co^{2+} ion exchange was experimentally studied on Zn-based IRMOF-1 and increased H_2, CH_4, and CO_2 uptakes of Co-IRMOF-1 with increasing Co^{2+} concentration were reported.[21] Zn-oxide-based MOFs are investigated due to their low toxicity and high gas storage capacities. Zhou et al.[22] synthesized a Zn-BTC type MOF, which could not adsorb any CO_2 and N_2 due to pore shrinkage upon activation, whereas 96% metal ion exchange of Zn^{2+} with Cu^{2+} led to N_2 (CO_2) adsorption capacity up to 325 (∼75) cm^3/g at 77 K (273 K).

Although experimental measurements have been performed for commonly studied MOFs, our knowledge on the gas adsorption mechanisms of MOFs upon metal exchange is still limited. To understand the molecular origins of gas adsorption mechanisms on M-MOFs, molecular simulations have been performed but only for a few materials. Yuan et al.[23] performed grand canonical Monte Carlo (GCMC) simulations for adsorption and separation of an equimolar CO_2/H_2 mixture on M-SIFSIX-3, where M = Cu, Zn, and Fe, and found that CO_2 molecules adsorb preferentially closer to the SIF^{2-} anion, whereas H_2 molecules prefer to adsorb at the pore center. CO_2/H_2 selectivities of Cu, Zn, and Fe-SIFSIX-3 were computed as 300, 400, and 500, respectively, at 10 bar, 298 K. Borycz et al.[13] investigated the change in the CO_2 affinity of Mg-, Ca-, Fe-, Cu-, Ge-, Sr-, Cd-, Sn-, and Ba-exchanged IRMOF-10 using ab initio calculations and molecular modeling. Due to the larger ionic radii of Ba^{2+}, the metal center had stronger interactions with the CO_2 compared to other metals, leading to high binding energies, and three times more CO_2 molecules near the metal center compared to original IRMOF-10. Recently, our group performed GCMC simulations on M-HKUST-1 and M-HATGUF (M = Cd, Co, Cr, Cu, Fe, Mn, Mo, Ni, Ru, and Zn) and showed that Cr-HKUST-1 and Cd-HKUST-1 have 11 and 38% enhanced CO_2/H_2 selectivities in addition to 27 and 60% enhanced adsorbent performance scores (APS) compared to the original Cu-HKUST-1.[24] As this literature review shows, studies focusing on the mixture gas adsorption and/or separation performance of M-MOFs are very scarce. Existing studies have focused only on commercial MOFs due to the fact that choosing the ideal MOF that will have a much-enhanced gas separation performance upon the metal exchange is challenging and the large diversity of MOF structures necessitates an initial screening of thousands of available materials.

Coordination geometry of the metal nodes, size and shape of the linkers, and topology of the framework play an important role in the extent of metal exchange.[25] Considering the fact that most of the synthesized MOFs to date have nodes with the Zn metal,[26,27] understanding their gas separation performance upon metal exchange is required to pave the way for achieving better performing materials. Therefore, in this work, we proposed a methodology to select the most appropriate material candidates for metal exchange among the MOFs having Zn-oxide nodes and investigated the influence of metal exchange on their CO_2/H_2 and CO_2/CH_4 mixture separation performances. We systematically categorized 10,221 MOFs according to their metal nodes, coordination of organic linkers, and the shape of the metal cluster. After this categorization, we focused on (i) two IRMOFs that have the same chemical building blocks, but the change of synthesis conditions results in MOFs with different crystal geometries (cubic vs hexagonal) due to the presence/absence of catenation, and (ii) two ZnO-MOFs with and without the guest ions incorporated to the MOF structure. Metal atoms (Zn) of these four MOFs were exchanged with M = Cd, Co, Cr, Cu, Mn, Ni, Ti, and V to examine 32 unique M-MOFs both for CO_2/H_2 and CO_2/CH_4 mixture separations. Gas separation performances of M-MOFs computed under pressure swing adsorption (PSA) and vacuum swing adsorption (VSA) conditions were then compared with those of the most recently reported IRMOFs and ZnO-MOFs. The relationship between the calculated performance metrics of in-silico-designed M-MOFs and their physical (pore size, surface area, and porosity) and chemical (partial charge of the metal atom) properties were examined. The investigation of gas−MOF and gas−gas interaction energies, as well as the preferential adsorption sites of gas molecules in the framework provided a molecular level understanding of the impact of metal exchange on gas separation performances of MOFs. These results will guide the future computational and experimental studies on M-MOFs to generate materials with superior CO_2/H_2 and CO_2/CH_4 separation performances.

2. COMPUTATIONAL METHODS

2.1. Classification and Selection of MOFs for In Silico Metal Exchange. We recently performed high-throughput computational screening of 10,221 MOFs retrieved from the Cambridge Structural Database (CSD)[28] for CO_2/H_2 separation and showed that MOFs perform well as CO_2 adsorbents.[29] In this work, we first utilized CSD ConQuest software[30] and conducted a connectivity search on these 10,221 MOFs. The guidelines described in the literature[27] were followed for targeted classification of MOFs, and 933 MOFs with Zn-oxide nodes were identified. These 933 MOFs were further narrowed down to 769 MOFs after excluding the MOFs that have functional groups and/or more than one type of organic linker. Complete metal-exchange of MOFs severely depends on factors such as the pore size distribution and flexibility of the framework, framework stability, coordination geometry of the metal node, and steric hindrance caused by the linkers.[25] We aimed to work on relatively simple MOF structures and eliminated the MOFs consisting of mixed linkers and/or functional groups due to the following reasons: (i) MOFs designed with mixed linker strategies can have defects,[31,32] or differing topologies and crystal structures,[33] but we aimed to work on MOFs with similar topologies after metal exchange and with a defect-free, homogeneous adsorption surface. (ii) MOFs with functional groups can have strong

https://doi.org/10.1021/acs.jpcc.1c03630
J. Phys. Chem. C 2021, 125, 17311−17322

electrostatic interactions with CO_2 as shown in our previous works[29,34] but we aimed to isolate the influence of metal exchange on CO_2/H_2 and CO_2/CH_4 selectivity by omitting the MOFs with functional groups and mixed linkers. 769 MOFs with Zn-oxide nodes, a single type of linker, and no functional groups were divided into two final subgroups depending on the shape of the metal cluster (coordination of the node): 140 IRMOF-like MOFs (IRMOFs) and remaining (629) MOFs with Zn-oxide nodes (ZnO-MOFs). The main difference between IRMOF-like and ZnO-MOFs is the shape of the metal cluster.[27] MOFs with IRMOF-like structures have a 4-connected configuration with oxygen atoms connected to each metal site as shown in Figure S1a, while MOFs with ZnO-MOF type structures have two metal atoms connected with four oxygen and one Zn atom bonded with six oxygen as shown in Figure S1b.This classification methodology is shown in Figure 1 together with the representative MOFs selected for

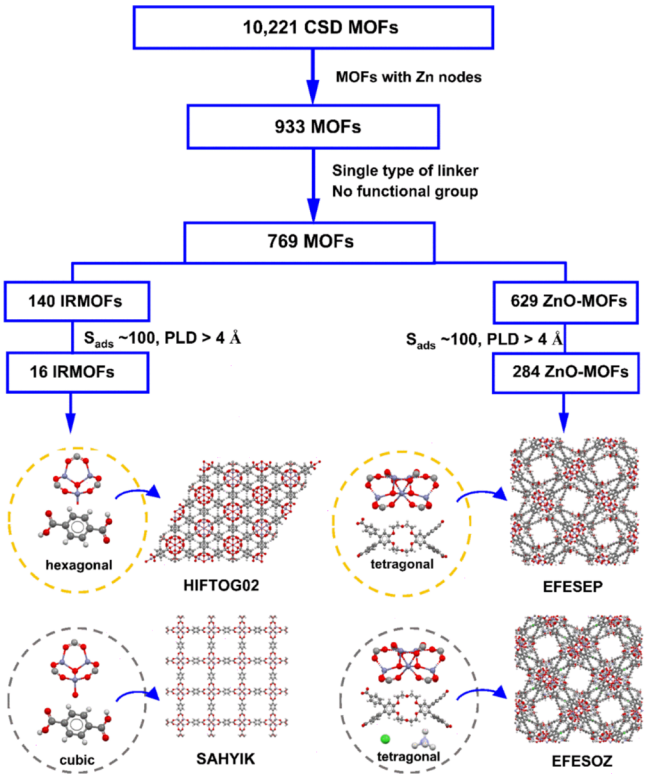

Figure 1. Targeted MOF categorization according to the type of node and building blocks to select the representative MOFs for in silico metal exchange. Carbon, oxygen, hydrogen, zinc, chlorine, and nitrogen are represented with gray, red, white, purple, green, and light blue colors, respectively.

metal exchange from IRMOFs and ZnO-MOFs. Representative MOFs from IRMOFs and ZnO-MOFs, which satisfy the following two criteria, were selected for metal exchange: (i) MOFs with pore limiting diameter (PLD) > 4 Å to avoid pore sizes smaller than or very close to the size of the gas molecules after geometry optimization, (ii) MOFs with CO_2/H_2 mixture selectivity (S_{ads}) ~ 100 at 1 bar, because these materials can have outstanding separation performances upon an increase in their CO_2 uptakes with metal exchange. We also identified a peer-MOF for each selected MOF to compare the change in their gas separation performances upon the metal exchange. 16 IRMOFs and 284 ZnO-MOFs had pore sizes >4 Å and S_{ads} ~ 100.

Among 16 IRMOFs, HIFTOG02 (PLD: 4.15 Å, S_{ads}: 119) was selected because it has the same building blocks as SAHYIK (known as IRMOF-1 or MOF-5)[35] but arranged in a hexagonal crystal geometry unlike the cubic geometry of SAHYIK.[36] Although SAHYIK (PLD: 7.8 Å) has a low S_{ads}, 9.5 at 1 bar, it was selected as the peer for HIFTOG02 to compare the influence of catenation on MOF performance upon the metal exchange. Among 629 ZnO-MOFs, EFESEP (SNU-200) with a PLD of 6.13 Å and a S_{ads} of 160 was selected with its peer EFESOZ (PLD: 6.2 Å, S_{ads}: 160), which has the same crystal structure as EFESEP but with the guest ions Cl^- and NH_4^+,[37] to investigate the influence of the guest ions on the gas separation performances of the metal exchanged ZnO-MOFs.

We note that the coordination geometry of the node, steric hindrance exposed by the linkers, pore size, and the stability of the framework are the preliminary factors that we considered before selecting the candidate MOFs for metal exchange.[25] The four MOFs we considered in our work for metal exchange (SAHYIK, HIFTOG02, EFESEP, and EFESOZ) have been experimentally reported to be stable with mediocre pore sizes.[36,37] We considered pore sizes between 3.3 and 4 Å as small, 4 and 20 Å as mediocre, and 20 and 45 Å as large by following the convention used in our previous study.[29] We selected SAHYIK as a benchmark MOF because several previous works have both experimentally and computationally performed metal exchange on IRMOF series.[13,38−40] For example, Ti, V, Cr, Mn, Fe, and Ni variants of MOF-5 were experimentally reported via cation exchange.[38,39] HIFTOG02[36] is the catenated form of MOF-5, thus we assumed that a metal exchange procedure similar to that of MOF-5 can be easily implemented on this material. We selected SNU-200 variants, EFESEP and EFESOZ, because SNU-200[37] has Zn-oxide nodes in frequently observed coordination geometries (octahedral and tetrahedral), and in a previous work,[41] exchange of Zn with Pd, Cd, Cu, Ni, Co, Mn, and Cr has been experimentally reported for a structure, which has a similar type of node geometry.

To examine the impact of metal type on the CO_2/H_2 and CO_2/CH_4 separation performances of SAHYIK, HIFTOG02, EFESEP, and EFESOZ, we studied eight different metals, Cd, Cu, Co, Cr, Mn, Ni, Ti, and V, which are commonly employed in both computational and experimental metal exchange studies on MOFs,[12,13,39] and obtained 32 unique M-MOFs. Prior to metal exchange, bound and unbound solvent molecules were cleaned from structures and metal exchange and geometry optimization were performed with Materials Studio 2020.[42] Original metal (Zn) of the structures was modified using the "modify element" tool implemented in the Materials Studio, and energy of the structure was minimized with an ultrafine convergence tolerance of 10^{-5} kcal/mol. A smart algorithm was employed for geometry optimization with a maximum iteration of 1000 steps. Convergence tolerances for geometry optimization were set as 10^{-6} Å for the distance, 10^{-5} kcal/mol for energy, and 10^{-4} kcal/mol/Å for force. Unit cell parameters were allowed to relax during geometry optimization, which enabled the bonds between atoms of the MOF relax after the metal exchange step. Geometry optimized version of the original MOF is labeled as "opt" throughout the manuscript. More details of this method were described in our previous study.[24]

https://doi.org/10.1021/acs.jpcc.1c03630
J. Phys. Chem. C 2021, 125, 17311−17322

Structural properties of MOFs such as accessible surface area (S_{acc}), the largest cavity diameter (LCD), PLD, and porosity (ϕ) were calculated using the Zeo++ software version 0.3.0.[43] To calculate the accessible surface area, we used a N_2-sized (3.70 Å) probe, whereas a probe size of zero was used for the porosity calculations. The PLD and LCD of the MOFs were calculated via percolating a probe through the simulation cell,[43] and PLD is defined as the size of the largest probe molecule that can pass the simulation cell freely at least through a channel in the MOF without overlapping any atoms (largest free sphere), while LCD is the largest included sphere in the unit cell.

2.2. Calculation of Gas Uptakes and Separation Performances of MOFs. Following the geometry optimization of M-MOF series, GCMC simulations were performed using RASPA simulation software[44] (version 2.0.36) to obtain CO_2/H_2 and CO_2/CH_4 mixture uptakes. Universal force field was used for the framework atoms.[45] CO_2 was modeled as a three-site molecule with partial charges on each site,[46] H_2 was modeled as a single sphere,[47] and CH_4 was modeled using the TraPPE model as a unified sphere with van der Waals interactions.[48] Lorentz−Berthelot mixing rules were applied to define pairwise interactions between unlike atoms. Partial charges to framework atoms were assigned with the Q_{eq} (charge equilibration) method implemented in RASPA[49,50] because simulations performed with Q_{eq} charges reproduced the available experimental gas adsorption data for M-HKUST-1 (M = Cr, Co, Fe, Ru, and Ni Zn) as we previously reported.[24] We used the formal oxidation state for each metal as implemented in the charge equilibration module of the RASPA simulation code.[44,50] These correspond to a +2 oxidation state for Cd, Co, Cr, Cu, Mn, Ni, and Zn; and a +3 oxidation state for Ti and V. For GCMC simulations, 10,000 cycles for the initialization run and 10,000 cycles for the production run were used, and the average values of gas adsorption were taken from the production step. The isosteric heat of adsorption (Q_{st}) values for gas molecules were computed during GCMC simulations using the fluctuation method in RASPA.[44] Gas adsorption snapshots were taken from the last simulation cycle to represent an image of the equilibrium state of adsorption.

To represent industrial precombustion gas mixture, the mole fractions of CO_2 and H_2 were set as 0.15 and 0.85, respectively,[51] while for the CO_2/CH_4 mixture, an equimolar composition was considered representing the landfill gas.[52] Adsorption and desorption conditions were set as 10 (1) and 1 (0.1) bar to mimic the PSA (VSA) process, respectively, at 298 K. We examined adsorption-based gas separation performances of MOFs under PSA and VSA conditions using five different metrics, adsorption selectivity (S_{ads}), CO_2 working capacity (ΔN_{CO_2}), adsorbent regenerability (R %), and adsorbent performance score (APS). S_{ads} reflects the affinity of a material toward the more strongly adsorbed gas, which is CO_2 for both separations. ΔN_{CO_2} represents the amount of CO_2 that can be captured throughout each adsorbent regeneration cycle. APS merges S_{ads} and ΔN_{CO_2} to determine the best performing MOFs. R % is used to determine how much CO_2 can be regenerated at each adsorbent regeneration cycle. Details for the calculation of these metrics are given in Table 1. For an efficient adsorption-based separation process, adsorbent materials offering high selectivity and high working capacity that lead to high APS together with a good value of R % (generally >85%) are desired.

Table 1. Calculation of Adsorbent Performance Evaluation Metrics Used in This Work[a]

metric	formula
mixture adsorption selectivity	$S_{ads}^{mix} = \frac{N_{ads,CO_2}}{N_{ads,j}} / \frac{y_{CO_2}}{y_j}$
working capacity	$\Delta N_{CO_2} = N_{ads,CO_2} - N_{des,CO_2}$
APS	$APS = S_{ads}^{mix} \times \Delta N_{CO_2}$
percent regenerability	$R\ \% = \Delta N_{CO_2}/N_{ads,CO_2} \times 100\%$

[a]$N_{ads,i}$: gas uptake under adsorption conditions (mol/kg), $N_{des,i}$: gas uptake under desorption conditions (mol/kg), y: bulk composition of the gas mixture, and j: H_2 or CH_4.

3. RESULTS AND DISCUSSION

3.1. Effect of Metal Exchange on CO_2/H_2 Uptakes of MOFs. We first compared the effect of metal exchange on CO_2/H_2 mixture uptakes of IRMOFs and ZnO-MOFs. We discussed the performances of MOFs with respect to their structural properties and the largest charge (LC) assigned to the metal atom. CO_2 and H_2 uptakes of 140 IRMOFs and 629 ZnO-MOFs computed at 0.1, 1, and 10 bar are shown in Figure 2. We color-coded and scaled the size of the data points according to the LC assigned to the framework atoms and PLD of the MOFs, respectively. Most of the IRMOFs and ZnO-MOFs had LC between 0.4 and 0.8 e^-, and IRMOFs had relatively larger pores (PLD range: 3.9−25.1 Å, LCD range: 5.5−26.1 Å) compared to ZnO-MOFs (PLD range: 3.7−19.2 Å, LCD range:4.2−21.6 Å). CO_2 uptakes of ZnO-MOFs were higher than those of IRMOFs at 0.1, 1, and 10 bar, while IRMOFs had slightly higher H_2 uptakes than ZnO-MOFs as pressure increased. Therefore, without metal exchange, ZnO-MOFs were potentially more promising in terms of their CO_2 capture performance from the CO_2/H_2 mixture compared to IRMOFs. IRMOFs and ZnO-MOFs with small pore sizes (shown with the smallest symbols) generally had the highest CO_2 uptakes at all pressures as shown in Figure 2a−f. In MOFs having small pores, CO_2 molecules have increased interactions with the framework atoms due to the strong confinement.[53] We note that most of the IRMOFs and ZnO-MOFs had small pore sizes and low LCs, and metal exchange can intensify the CO_2-MOF interactions, making these materials promising with high CO_2 uptakes.

The CO_2 and H_2 uptakes of M-MOFs that we focused on are also shown in Figure 2. For the group of IRMOFs, we compared the gas adsorption performances of M-HIFTOG02 (stars) and M-SAHYIK (triangles) with 140 IRMOFs (circles) in Figure 2a−c. The ranges of PLD for M-HIFTOG02 and M-SAHYIK were computed as 4.1−4.6 and 7.8−8.2 Å, respectively. M-HIFTOG02 is the catenated form of M-SAHYIK,[36] therefore the former series had narrower pore sizes, smaller S_{acc}, and lower porosity than the latter (given in Table S1). As shown in Figure 2a−c, the metal exchange in M-HIFTOG02 had a strong influence on the CO_2 uptakes, while H_2 uptakes remained almost the same. We observed the greatest improvement in the CO_2 uptake of M-HIFTOG02 at 0.1 bar (Figure 2a), where CO_2 uptake of the original Zn-HIFTOG02 increased from 0.08 mol/kg to 0.18, 0.21, 0.34, and 0.52 mol/kg for Cr, Ti-, Ni-, and V-HIFTOG02, respectively. Ti, Ni, Cr, and V had the highest LC (1.40,

https://doi.org/10.1021/acs.jpcc.1c03630
J. Phys. Chem. C 2021, 125, 17311−17322

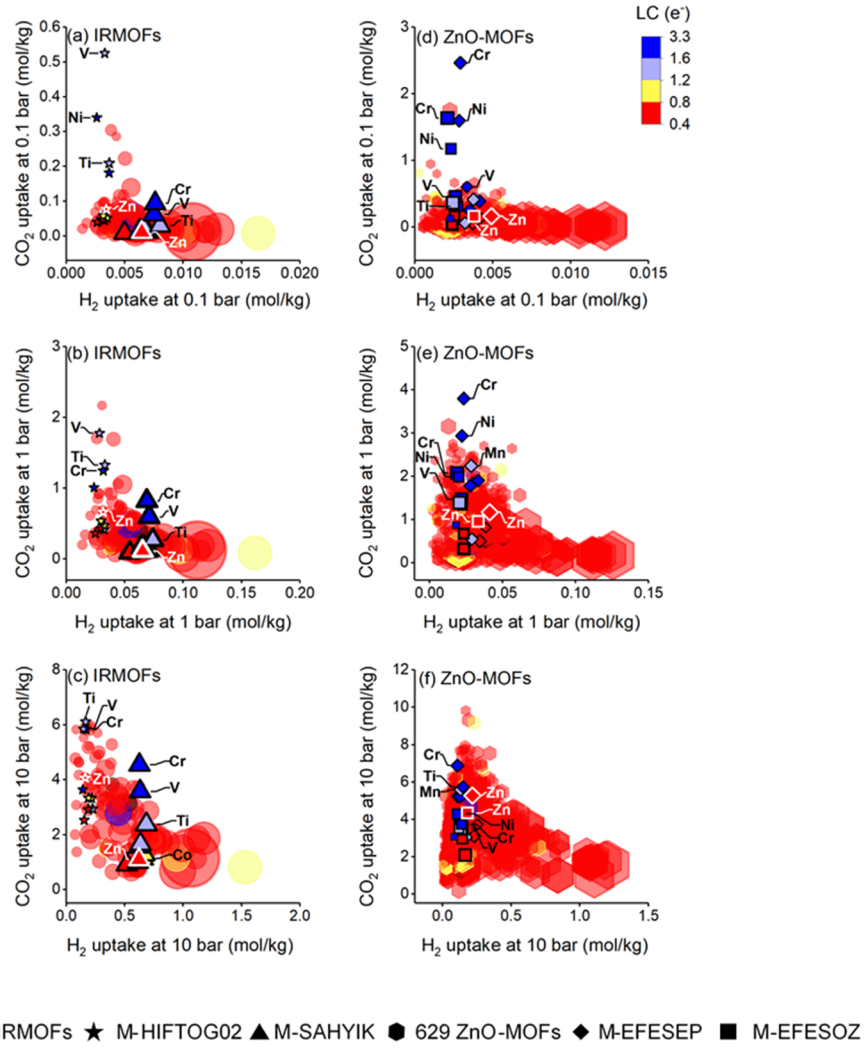

Figure 2. (a–c) CO_2 and H_2 uptakes of 140 IRMOFs (circles), M-HIFTOG02 (stars), and M-SAHYIK (triangles) at 0.1, 1, and 10 bar. (d–f) CO_2 and H_2 uptakes of 629 ZnO-MOFs (hexagonals), M-EFESEP (diamonds), and M-EFESOZ (squares) at 0.1, 1, and 10 bar. Color and size of symbols represent the LC and PLD of MOFs, respectively.

1.58, 2.07, and 2.33 e^- for Ti, V, Cr, and Ni, respectively) among the M-HIFTOG02 series. Because CO_2-MOF electrostatic interactions are important at low pressures,[53] high LCs of these metals led to enhanced CO_2 uptakes in these MOFs. Thus, at 0.1 bar, CO_2 uptakes of V-HIFTOG02 and Ni-HIFTOG02 even exceeded those of all IRMOFs. The effect of metal exchange on the CO_2 uptakes of M-IRMOFs was weaker but still observable at 10 bar compared to 0.1 bar. At 10 bar, Ti-HIFTOG02 with an exceptional CO_2 uptake of 6.12 mol/kg surpassed the CO_2 uptakes of all IRMOFs. This is a significant finding because the IRMOF with the highest CO_2 uptake in our subset had a CO_2 uptake value of 5.94 mol/kg and Ti-HIFTOG02 surpassed even this limit. This demonstrates that by exchanging Zn with V and Ti, we can build MOFs with exceptional CO_2 uptakes that exceed the upper limits of CO_2 uptake for all the existing IRMOFs.

Zn-SAHYIK had higher H_2 uptakes and lower CO_2 uptakes compared to Zn-HIFTOG02. CO_2 uptakes of SAHYIK increased up to nine times, from 0.01 mol/kg to 0.09 mol/kg at 0.1 bar, when Zn is exchanged with Cr and the CO_2 uptake of Cr-SAHYIK even overcame the CO_2 uptake of Zn-HIFTOG02. However, the upper limit for CO_2 uptakes of M-SAHYIK was lower than that of M-HIFTOG02, as catenated MOFs (M-HIFTOG02 in this work) have been shown to have higher CO_2 adsorption due to increased framework densities and lower porosities when compared to their noncatenated counterparts (M-SAHYIK in this work).[29,54] This can be supported with the higher Q_{st,CO_2} values that we calculated for M-HIFTOG02 (ranging from −23 to −37 kJ/mol) than those for M-SAHYIK (ranging from −13 to −29 kJ/mol) at 0.1 bar. At 1 bar and 10 bar (Figure 2b,c), CO_2 uptakes of M-SAHYIK almost reached those of M-HIFTOG02. At high pressures, the impact of physical properties such as the surface area and porosity of MOFs on gas uptakes is more pronounced.[55] M-HIFTOG02 series were easily saturated with CO_2 molecules due to their lower porosities and surface areas (as shown in Table S1) compared to M-SAHYIK series, which have larger pores and a higher surface area providing more space for gas adsorption.

We compared the gas adsorption performances of M-EFESEP (diamonds) and M-EFESOZ (squares) with those of 629 ZnO-MOFs (hexagonals) in Figure 2d–f. Similar to M-IRMOFs, metal exchange did not remarkably change the H_2 uptakes of M-ZnO-MOFs but altered their CO_2 uptakes. As shown in Figure 2d, high LC assigned to Cr-EFESEP and Cr-EFESOZ provided the maximum CO_2 uptakes observed for

https://doi.org/10.1021/acs.jpcc.1c03630
J. Phys. Chem. C 2021, 125, 17311−17322

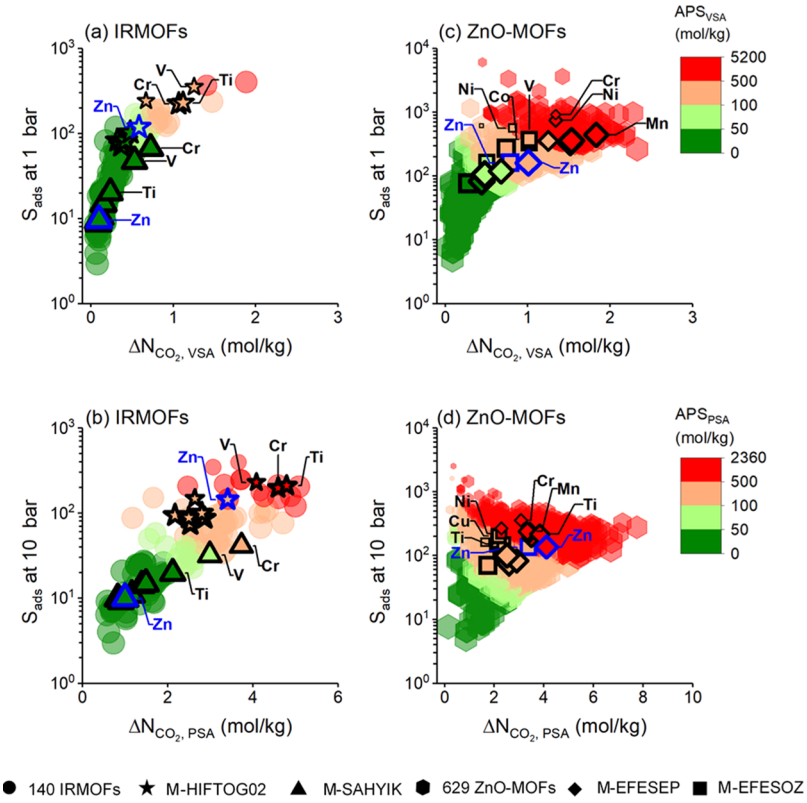

Figure 3. (a,b) ΔN_{CO_2} and S_{ads} of M-HIFTOG02 (stars), M-SAHYIK (triangles), and 140 IRMOFs (circles), (c,d) ΔN_{CO_2} and S_{ads} of M-EFESEP (diamonds), M-EFESOZ (squares), and 629 ZnO-MOFs (hexagonals) are shown for CO_2/H_2 mixture separation under VSA and PSA conditions. Size of symbols represents *R* %, color of symbols represents APS under the corresponding working conditions.

both the M-EFESEP and M-EFESOZ series, followed by Ni and V. With Cr-EFESEP (Cr-EFESOZ), CO_2 uptakes increased by 15 (10)-fold compared to the original Zn-EFESEP (Zn-EFESOZ) at 0.1 bar. Smaller PLDs of M-EFESEP (3.9−6.1 Å) lead to slightly higher CO_2 uptakes compared to M-EFESOZ (PLD: 3.7−6.8 Å). Due to the presence of guest ions in the pores of M-EFESOZ, it had a smaller surface area compared to M-EFESEP (given in Table S2), therefore the available space for CO_2 and H_2 molecules was less in M-EFESOZ compared to that in M-EFESEP. Moreover, the presence of anions (Cl^-) has been shown to reduce CO_2−CO_2 interactions,[56] both Lennard Jones (LJ) and Coulomb, in the narrow pores of M-EFESOZ, which lead to lower CO_2 adsorption compared to M-EFESEP. For example, changing the metal from Zn to Cr increased the CO_2 uptake of M-EFESEP from 0.17 to 2.47 mol/kg at 0.1 bar, while for M-EFESOZ, the CO_2 uptake increased from 0.16 to 1.63 mol/kg. The CO_2 uptake of Cr-EFESEP is even higher than the CO_2 uptakes of all ZnO-MOFs at 0.1 bar. At 1 bar (Figure 2e), Cr still had a positive impact on the CO_2 uptakes, and CO_2 uptake of Zn-EFESEP (Zn-EFESOZ) increased from 1.17 to 3.80 mol/kg (from 0.95 to 2.07 mol/kg) when Cr was used. At 10 bar, exchanging Zn with Cr in EFESEP slightly increased CO_2 uptake from 5.28 to 6.88 mol/kg (Figure 2f).

We compared the increase in CO_2 uptakes of M-IRMOFs and M-ZnO-MOFs between 0.1 and 10 bar. At low pressure, CO_2 uptakes of M-ZnO-MOFs were found to be more affected from the metal exchange compared to M-IRMOFs. For example, at 0.1 bar, CO_2 uptake of M-HIFTOG02, increased up to 7-fold when Zn was exchanged with V (Figure 2a), whereas CO_2 uptakes of M-EFESEP increased up to 15-fold when Zn was exchanged with Cr (Figure 2d). The surface area and porosity of MOFs, and proximity of gas molecules to metal centers became important factors in determining the gas adsorption properties of M-MOFs with increased pressure.[13] At 10 bar, with the enhancement in the CO_2 uptake, Ti-HIFTOG02 surpassed all IRMOFs (Figure 2c), while Cr-EFESEP and Cr-EFESOZ surpassed most of the ZnO-MOFs (Figure 2f). Overall, we observed that exchange of Zn with Cr significantly increased the CO_2 uptakes of both M-IRMOFs and M-ZnO-MOFs.

To explain the change in the gas uptakes of MOFs upon the metal exchange, we examined the contribution of LJ interaction energies (E_{LJ}) for MOF-H_2, MOF-CO_2, CO_2−CO_2, H_2−H_2, and CO_2−H_2, and the contribution of the Coulombic interaction energies ($E_{Coulomb}$) for MOF-CO_2 and CO_2−CO_2 to the total energy. Figure S2 shows that the highest contributions to total energy were by $E_{LJ,MOF\text{-}CO_2}$ and $E_{Coulomb,MOF\text{-}CO_2}$ for M-SAHYIK and M-HIFTOG02, while the gas−gas interaction energies E_{LJ,H_2-H_2} and E_{LJ,CO_2-H_2} had almost no contribution at any pressure. MOF-H_2 LJ interaction energy, $E_{LJ,MOF\text{-}H_2}$, in M-SAHYIK was more effective compared to that in M-HIFTOG02 (Figure S2a−c), which can be explained by the size and geometry of the structures. Large rectangular pores of M-SAHYIK did not favor CO_2 adsorption as much as small triangular pores of M-HIFTOG02, which resulted in lower MOF-CO_2 interaction energies and higher MOF-H_2 interaction energies. Thus, higher H_2 adsorption was observed in M-SAHYIK (0.05−0.07 mol/kg) compared to M-HIFTOG02 (0.02−0.03 mol/kg) at 1 bar. As pressure increased from 0.1 to 10 bar, contribution of $E_{Coulomb,MOF\text{-}CO_2}$

https://doi.org/10.1021/acs.jpcc.1c03630
J. Phys. Chem. C 2021, 125, 17311−17322

in M-HIFTOG02 decreased, whereas contributions of $E_{LJ,MOF\text{-}CO_2}$ and E_{LJ,CO_2-CO_2} increased as shown in Figure S2d–f. This was due to the presence of a high CO_2 loading in the pores of M-HIFTOG02 at 10 bar, which can be observed from the adsorption snapshots given in Figure S3. The contribution of $E_{Coulomb,MOF\text{-}CO_2}$ to the total energy was higher for V, Ni, Ti, and Cr-exchanged versions of M-SAHYIK and M-HIFTOG02 as the higher LC enhanced the calculated CO_2-MOF electrostatic interactions compared to those in Zn-SAHYIK and Zn-HIFTOG02. In Figure S4, a slightly higher contribution of E_{LJ,CO_2-CO_2} and $E_{Coulomb,CO_2-CO_2}$ to total interaction energy in M-EFESEP compared to M-EFESOZ is shown. Simulation snapshots shown in Figure S5 also indicate that all pores provide adsorption sites in M-EFESEP, whereas in M-EFESOZ mainly the large pore was preferred by both gases. As a result, MOFs with V, Ti, Ni, and Cr, which have LC > 1.4 e^- and PLD < 5 Å led to a stronger confinement of CO_2 at low pressure, as supported by a high contribution of $E_{Coulomb,MOF\text{-}CO_2}$ to total interaction energy, and as a result these MOFs had the highest CO_2 uptakes (the largest improvement in CO_2 uptake was observed for Cr-EFESEP, from 0.17 to 2.47 mol/kg at 0.1 bar). As the pressure increased to 10 bar, Cr-EFESEP had the highest CO_2 uptake with the improvement from 5.28 to 6.88 mol/kg, followed by Ti-HIFTOG02 with the improved CO_2 uptake from 4.06 to 6.12 mol/kg. This increase was attributed to the tight packing of CO_2 molecules inside the MOF pores as shown by decreased $E_{Coulomb,MOF\text{-}CO_2}$ and increased $E_{LJ,MOF\text{-}CO_2}$, E_{LJ,CO_2-CO_2}. Overall, MOFs with V, Ti, Ni, and Cr metals in M-HIFTOG02 series had higher CO_2 uptakes than M-SAHYIK series at all pressures due to the catenated structure of M-HIFTOG02, and MOFs with V, Ti, Ni, and Cr in M-EFESEP series had higher CO_2 uptakes than M-EFESOZ series due to the empty space left by the absence of guest ions.

3.2. Effect of Metal Exchange on CO_2/H_2 Separation Performances of MOFs. The ultimate goal of our work was to determine the effect of metal exchange on the adsorption-based gas separation performances of MOFs. In Figure 3, S_{ads} and ΔN_{CO_2} of IRMOFs and ZnO-MOFs for CO_2/H_2 mixture separation were shown under VSA and PSA conditions. Effects of metal exchange on APS were shown with the color of the symbols and adsorbent regenerability (R %) was shown with the size of the symbols in Figure 3. Under VSA and PSA conditions, ZnO-MOFs had higher adsorption selectivity (S_{ads}) and CO_2 working capacity (ΔN_{CO_2}), than IRMOFs, which was expected due to the higher CO_2 uptakes of ZnO-MOFs. As Figure 3a,b shows, M-HIFTOG02 materials (stars) had higher S_{ads} and ΔN_{CO_2} compared to M-SAHYIK series (triangles). S_{ads} and ΔN_{CO_2} of original Zn-HIFTOG02 were computed as 119 and 0.58 mol/kg, respectively, whereas with changing the metal from Zn to V, S_{ads} and ΔN_{CO_2} increased to 355 and 1.25 mol/kg, respectively, leading to a 6-fold increase in APS under VSA conditions. Under PSA conditions, V and Ti increased the S_{ads} of Zn-HIFTOG02 from 144 to 229 and 211, respectively, while its ΔN_{CO_2} increased from 3.4 to 4 and 4.79 mol/kg, respectively. A trade-off between S_{ads} and ΔN_{CO_2} has been commonly observed for MOFs with different physical properties,[57] whereas here we showed that S_{ads} and ΔN_{CO_2} can be improved simultaneously with metal exchange. We also considered the change in R % values upon the metal exchange because R % is a significant metric for the efficiency of adsorbents in cyclic processes. All M-HIFTOG02 except Ni-HIFTOG02 had R % values equal to or larger than 70%, which is a good range of R % values for an industrial gas separation process.

Exchange of Zn with Cr in M-SAHYIK (triangles) increased the S_{ads} of Zn-SAHYIK from 10 to 67 at 1 bar, and from 10 to 41 at 10 bar, in addition to an enhanced ΔN_{CO_2} from 0.1 to 0.7 mol/kg under VSA conditions, and from 1 to 3.7 mol/kg under PSA conditions as shown in Figure 3. Therefore, upon the metal exchange, APS of Cr-SAHYIK increased 50 times under VSA conditions, and 15 times under PSA condition compared to the APS of Zn-SAHYIK. M-SAHYIK series also preserved their high R % (represented by the size of the triangles) under VSA conditions upon the metal exchange, which made them highly promising materials. Overall, the metal exchange had a greater impact on the adsorbent performance evaluation metrics of M-SAHYIK than M-HIFTOG02, and the separation performance of Cr-SAHYIK even approached to that of Zn-HIFTOG02 in terms of both S_{ads} and ΔN_{CO_2} under VSA conditions, and in terms of ΔN_{CO_2} under PSA conditions. At this point, we compared the performances of M-SAHYIK and M-HIFTOG02, which had the highest APS and R % >70% with the performances of all IRMOFs. Under VSA (PSA) conditions, APS of V-HIFTOG02 is higher than 98% (98%) of all IRMOFs, whereas APS of Cr-SAHYIK is higher than 85% (75%) of all IRMOFs, indicating that metal exchange significantly extended the current adsorbent performance limits of IRMOFs under VSA and PSA conditions.

In Figure 3c,d, S_{ads} and ΔN_{CO_2} trends of M-EFESEP (diamonds) and M-EFESOZ (squares) were compared with the results of ZnO-MOFs (hexagonals) under VSA and PSA conditions. Under VSA conditions, both S_{ads} and ΔN_{CO_2} of Zn-EFESEP and Zn-EFESOZ were improved with the metal exchange, while the improvement in S_{ads} was more pronounced compared to the improvement in ΔN_{CO_2}. Changing the metal from Zn to Cr increased S_{ads} of EFESEP six times (from 161 to 921) and of EFESOZ four times (from 160 to 613) under VSA conditions. Moreover, Zn-EFESEP exhibited ΔN_{CO_2}, S_{ads}, and R % of 1.01 mol/kg, 160, and 86%, respectively, whereas Mn-EFESEP led to a more promising combination of ΔN_{CO_2}, S_{ads}, and R % as 1.83 mol/kg, 446, and 81%, respectively, under VSA conditions. Similarly, ΔN_{CO_2}, S_{ads}, and R % values of Zn-EFESOZ were computed as 0.79 mol/kg, 160, and 83%, and these values were improved to 1.02 mol/kg, 378, and 74%, respectively, for Co-EFESOZ. We note that the metal exchange with Cr increased the APS of Zn-EFESEP exceptionally from 162 to 1233 mol/kg, while Ni increased the APS of Zn-EFESOZ from 126 to 462 mol/kg, under VSA conditions. Upon the exchange of Zn with V, Ni, and Cr, a decrease was observed in ΔN_{CO_2} of M-EFESEP and M-EFESOZ under PSA conditions, which was due to the more significant increase in their CO_2 uptakes upon metal exchange at 1 bar compared to at 10 bar. However, with the increase in the S_{ads} (from 137 to 359), APS of Zn-EFESEP increased from 562 to 1104 mol/kg with Cr under PSA conditions. Overall, metal-exchange with Cr, Ni, and V led to a good combination of ΔN_{CO_2} and S_{ads} for M-EFESEP and M-EFESOZ under VSA conditions, while under PSA conditions an improvement in S_{ads} was achievable.

https://doi.org/10.1021/acs.jpcc.1c03630
J. Phys. Chem. C 2021, 125, 17311−17322

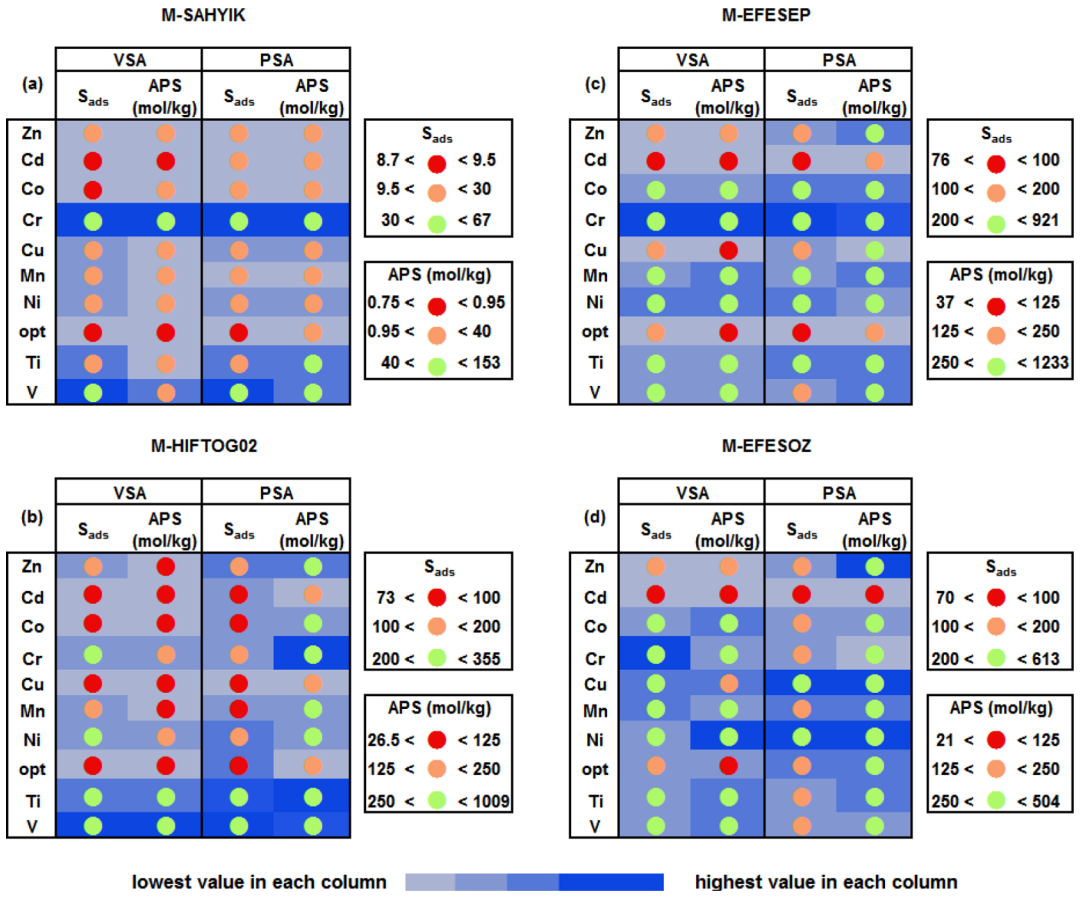

Figure 4. Infographic representing the effect of metal exchange on S_{ads} and APS of (a) M-SAHYIK, (b) M-HIFTOG02, (c) M-EFESEP, and (d) M-EFESOZ for CO_2/H_2 mixture separation under VSA and PSA conditions. "opt" represents the "geometry optimized version of the original MOF".

It is important to compare the calculated CO_2 uptake and CO_2/H_2 selectivity of the M-MOFs with those of existing MOFs constructed from the same metals to better situate the results of our work. Gagliardi and co-workers investigated single-component CO_2 adsorption in M-IRMOF-10 (M = Mg, Ca, Fe, Cu, Zn, Ge, Se, Cd, Sn, and Ba) and compared the CO_2 adsorption isotherms of M-IRMOF-10 with IRMOF-1, IRMOF-7, IRMOF-16, and MOF-200.[13] At 1 bar, 298 K, single-component CO_2 uptake of the best performing M-MOF (Ba-IRMOF-10) was computed as 1.9 mol/kg; while IRMOF-10, IRMOF-1, IRMOF-7, IRMOF-16, and MOF-200 had CO_2 uptakes of 0.8, 1.82, 1.79, 0.56, and 0.59 mol/kg, respectively. In this study, we computed the highest CO_2 uptake with Cr-SAHYIK (Cr-IRMOF-1) as 0.82 mol/kg. We note that this CO_2 uptake was computed for a CO_2/H_2: 15/85 bulk mixture at 1 bar, 298 K, therefore the performance of Cr-SAHYIK can be considered as promising. We compared the CO_2 uptake and CO_2/H_2 selectivity of the top MOFs identified in this work with those of the top candidates of M-HKUST-1 series, where M = Cd, Co, Cr, Cu, Fe, Mn, Mo, Ni, Ru, and Zn in our previous study.[24] At 1 bar, 298 K, Cr-HKUST-1 had a CO_2 uptake of 0.82 mol/kg and a selectivity of 97.63, while at 10 bar, 298 K, Cr-HKUST-1 was one of the top performers among other metal exchanged M-HKUST-1 with a CO_2 uptake of 4.29 mol/kg and a selectivity of 67.75. In this work, Cr-EFESEP had the highest CO_2/H_2 selectivity and CO_2 uptake of 921.25 and 3.8 mol/kg, respectively, at 1 bar, 298 K, and 358.72 and 6.88 mol/kg, respectively, at 10 bar, 298 K. These comparisons showed that metal exchange in Zn-MOFs led to superior performances compared to the performances of M-HKUST-1 for CO_2/H_2 mixture separation.

Finally, in Figure 4, we summarized the overall effect of metal exchange on the CO_2/H_2 separation performances of M-SAHYIK, M-HIFTOG02, M-EFESEP, and M-EFESOZ series under VSA and PSA conditions. The intensity of the blue color shifting from low to high represents the improvement in S_{ads} or APS, while the color of the circles reflects the most promising (green), the least promising (red), and in-between (yellow) performances (S_{ads} or APS) of M-MOFs. Figure 4a represents that exchange of Zn with Cr in M-SAHYIK increased both S_{ads} and APS under VSA and PSA conditions, and this was followed by V, uplifting the performance of Zn-SAHYIK to one of the highest performances. Similarly, changing the metal from Zn to Cr, Mn, or Ni enhanced the S_{ads} and APS of M-HIFTOG02 under VSA conditions, while Ti increased the APS of M-HIFTOG02 as much as Cr under PSA conditions as shown in Figure 4b. For M-EFESEP, significant improvements in the S_{ads} and APS under VSA and PSA conditions were observed when the original metal (Zn) was changed to V or Ti as shown in Figure 4c. As shown in Figure 4d, for M-EFESOZ exchange of Zn with a wide range of metals, Co, Cr, Mn, Ni, Ti, and V could double S_{ads} and APS of the MOF. These findings suggest that a major improvement in the gas separation efficiency of MOFs can be obtained by changing the metal from Zn to especially Cr or V, therefore, the

https://doi.org/10.1021/acs.jpcc.1c03630
J. Phys. Chem. C 2021, 125, 17311−17322

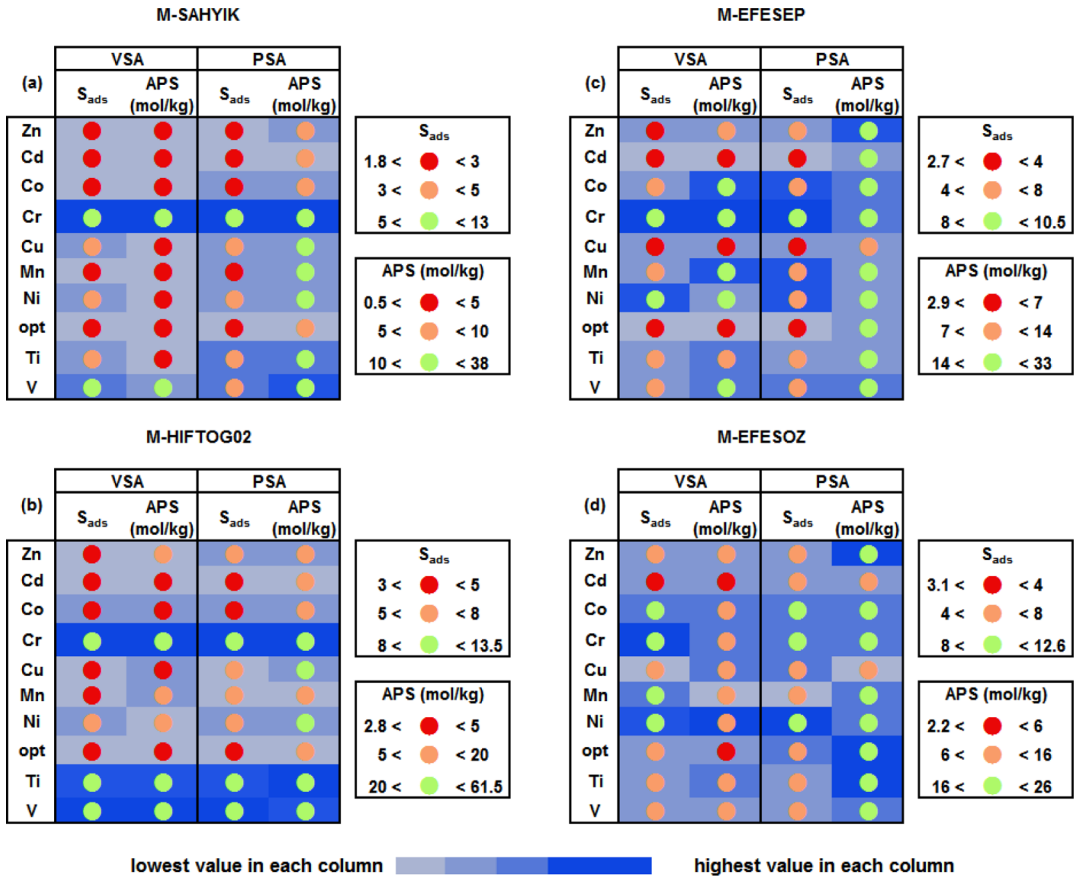

Figure 5. Infographic representing the effect of metal exchange on S_{ads} and APS of (a) M-SAHYIK, (b) M-HIFTOG02, (c) M-EFESEP, and (d) M-EFESOZ for CO_2/CH_4 mixture separation under VSA and PSA conditions. "opt" represents the "geometry optimized version of the original MOF".

synthesis and/or postsynthetic modification of MOFs with these metals warrants further studies.

3.3. Effect of Metal Exchange on CO_2/CH_4 Separation Performances of MOFs. Because we obtained improved CO_2/H_2 separation performances with M-IRMOFs and M-ZnO-MOFs, we also tested their separation performances for an equimolar CO_2/CH_4 mixture. In Figure 5, we represented the effect of exchanging Zn with different metals on S_{ads} and APS of M-HIFTOG02, M-SAHYIK, M-EFESEP, and M-EFESOZ for CO_2/CH_4 separation under VSA and PSA conditions. As shown in Figure 5a,b, similar to CO_2/H_2 separation, superior S_{ads} and APS values were obtained with V- and Ti-HIFTOG02 compared to Zn-HIFTOG02 for CO_2/CH_4 separation under both conditions. With the improvement in its S_{ads}, Cr-SAHYIK had a similar S_{ads} compared to V-HIFTOG02 under VSA conditions. Zn-HIFTOG02 and Zn-SAHYIK had S_{ads} of 3.9 and 1.8, respectively, for CO_2/CH_4 separation under VSA conditions, which increased to 13.5 with V-HIFTOG02 and to 13.2 with Cr-SAHYIK. This is due to the significantly higher CO_2 uptakes and lower CH_4 uptakes of V-HIFTOG02 and Cr-SAHYIK compared to those of their Zn-versions as shown in Figure S6. For example, CO_2 uptake of Zn-HIFTOG02 increased from 0.25 to 1.06 mol/kg (~4 fold) with V and CO_2 uptake of Zn-SAHYIK increased from 0.04 to 0.33 mol/kg (~9 fold) with Cr at 0.1 bar. At 1 bar, CO_2 uptake of Zn-HIFTOG02 increased from 1.80 to 3.47 mol/kg (~2 fold) with V, and CO_2 uptake of Zn-SAHYIK increased from 0.36 to 2.39 mol/kg (~6 fold) with Cr. Thus, V-HIFTOG02 and Cr-SAHYIK significantly outperformed all IRMOFs under VSA conditions. This was followed by Cr- and Ni-HIFTOG02, and V-SAHYIK, which also had high CO_2 uptakes close to the maximum of the CO_2 uptakes of all IRMOFs. In Figure S7, we provided S_{ads} and ΔN_{CO_2} of M-IRMOFs and M-ZnO-MOFs for CO_2/CH_4 separation. As shown, both the selectivity and working capacity of MOFs increased with metal exchange. A remarkable increase in ΔN_{CO_2} of Zn-SAHYIK, from 0.33 to 2.06 mol/kg under VSA conditions, was observed when Cr was used. Both V-HIFTOG02 and Cr-SAHYIK had the highest APS values and surpassed the performances of all IRMOFs under VSA conditions. Under PSA conditions, V-HIFTOG02 and Ti-HIFTOG02 had outstanding separation performances compared to all IRMOFs, while Cr-SAHYIK competed with the best performing IRMOFs due to its high S_{ads}, ΔN_{CO_2}, and high APS.

For M-ZnO-MOFs, as shown in Figure S6, exchanging Zn with Cr increased the CO_2 uptake of Zn-EFESEP from 0.46 to 2.95 mol/kg, and of Zn-EFESOZ from 0.40 to 1.86 mol/kg, at 0.1 bar. Cr-EFESEP had a CO_2 uptake higher than that of all ZnO-MOFs at 0.1 bar. At 1 and 10 bar, metal exchange contributed less to CO_2 uptakes but was still distinctive, and Cr-EFESEP had as high CO_2 uptakes as the best performing ZnO-MOFs at 1 bar. As a result, Cr significantly increased the S_{ads} of Zn-EFESEP from 3.8 to 10.5 for CO_2/CH_4 separations and APS increased from 7.7 to 21.7 mol/kg under VSA conditions as shown in Figure 5c. Figure 5d shows that S_{ads} of Zn-EFESOZ increased from 4.1 to 12.6 when Zn was changed to Cr, and Cr-EFESOZ had a high S_{ads} close to the highest S_{ads}

https://doi.org/10.1021/acs.jpcc.1c03630
J. Phys. Chem. C 2021, 125, 17311−17322

observed for ZnO-MOFs (shown in Figure S7). Ni followed Cr and increased S_{ads} of Zn-EFESOZ from 4.1 to 11.3 under VSA conditions, while its APS also increased from 6.7 to 15.7 mol/kg. Although we selected the MOFs for in silico metal exchange by considering their pore sizes and S_{ads} for CO_2/H_2 separation, M-MOFs considered in this work performed well both for CO_2/H_2 and CO_2/CH_4 mixtures. We observed a significant increase in both S_{ads} and APS of MOFs especially when Zn was exchanged with V, Cr, and Ni. This is an important result signaling that the MOFs carefully selected for metal exchange for CO_2/H_2 separation can have improved separation performances also for other gas mixtures such as CO_2/CH_4.

Finally, it is important to note that the M-MOFs we examined in this work are hypothetically produced with computational methods and with the assumption of successful exchange of all metals in the framework. Combination of several factors, such as the MOF topology, coordination geometry of the metal node, pore sizes, and size and shape of the linkers, determines the extent of metal exchange of MOFs in experimental studies.[25] These factors may lead to partial metal exchange in MOFs, which eventually influence the CO_2 capture performance of materials. Our results can be considered as useful guidelines to achieve the upper limits of CO_2 separation performances of metal-exchanged M-IRMOFs and M-ZnO-MOFs under industrially applicable conditions for CO_2/H_2 and CO_2/CH_4 mixture separations.

4. CONCLUSIONS

In this study, we presented a methodology to identify the most promising MOFs, which have the potential to provide an outstanding CO_2 capture performance after metal exchange and evaluated their CO_2/H_2 and CO_2/CH_4 mixture separation performances. Out of 10,221 MOFs, we first identified 769 MOFs containing Zn nodes and a single type of linker without any functional groups (140 IRMOFs and 629 ZnO-MOFs), then targeted the MOFs providing $S_{ads} \sim 100$ and PLD > 4 Å (16 IRMOFs and 284 ZnO-MOFs) and selected the candidate MOFs and their peer MOFs for metal exchange (two IRMOFs, M-SAHYIK and M-HIFTOG02, and two ZnO-MOFs, M-EFESEP and M-EFESOZ). We exchanged the metal atom (Zn) of the selected four MOFs with eight different metals (Cd, Co, Cr, Cu, Mn, Ni, Ti, and V), and 32 unique M-MOFs (16 M-IRMOFs and 16 M-ZnO-MOFs) were obtained. Molecular-level insights obtained from atomically detailed simulations showed that higher contributions of MOF-CO_2 electrostatic interactions in MOFs with Cr, V, Ni, and Ti metals led to higher CO_2 uptakes. We compared the CO_2 separation performances of 32 in silico designed M-MOFs with those of 629 ZnO-MOFs and 140 IRMOFs. Our results showed that the most significant improvement in the CO_2/H_2 and CO_2/CH_4 selectivities of MOFs was obtained with Cr, V, Ni, and Ti metals. After the exchange of Zn with V, CO_2/H_2 selectivity of HIFTOG02 (355 at 1 bar) exceeded the selectivity of 138 out of 140 IRMOFs. The exchange of Zn with Cr improved the selectivity of EFESEP (921 at 1 bar) and surpassed the selectivities of 602 ZnO-MOFs out of 629 ZnO-MOFs. These increases in selectivities were accompanied by an increase in working capacity of MOFs resulting in improved APSs. Thus, metal exchange was shown to significantly extend the current adsorbent performance limits of ZnO-MOFs. We hope these results will inspire computational and experimental studies that investigate the influence of metal exchange on CO_2 separation performances of MOFs with different MOF topologies or a rich amount of guest ion pairs and will serve as a catalyst to identify novel M-MOFs with exceptional CO_2 capture performances.

■ ASSOCIATED CONTENT

Supporting Information

The Supporting Information is available free of charge at https://pubs.acs.org/doi/10.1021/acs.jpcc.1c03630.

Classification of MOF node types according to the bonding scheme for IRMOFs and ZnO-MOFs; contribution of LJ interaction energies and Coulomb interaction energies to total energy in M-SAHYIK, M-HIFTOG02, M-EFESEP, and M-EFESOZ; CO_2 and H_2 adsorption snapshots of Zn-SAHYIK, Cr-SAHYIK, Zn-HIFTOG02, V-HIFTOG02, Zn-EFESEP, Cr-EFESEP, Zn-EFESOZ, and Cr-EFESOZ at 10 bar; CO_2 and CH_4 uptakes of IRMOFs, ZnO-MOFs, M-IRMOFs, and M-ZnO-MOFs at 0.1, 1, and 10 bar; CO_2/CH_4 separation performances of IRMOFs, ZnO-MOFs, M-IRMOFs, and M-ZnO-MOFs under VSA and PSA conditions; and S_{ads} of M-IRMOFs and M-ZnO-MOFs at 0.1, 1, and 10 bar with respect to their physical properties (LCD, PLD, S_{acc}, and ϕ) and their chemical properties (ε, σ, and the LC assigned in the framework) (PDF)

■ AUTHOR INFORMATION

Corresponding Author

Seda Keskin − *Department of Chemical and Biological Engineering, Koc University, 34450 Istanbul, Turkey;* orcid.org/0000-0001-5968-0336; Phone: +90(212)338 1362; Email: skeskin@ku.edu.tr

Authors

Gokay Avci − *Department of Materials Science and Engineering, Koc University, 34450 Istanbul, Turkey*

Cigdem Altintas − *Department of Chemical and Biological Engineering, Koc University, 34450 Istanbul, Turkey*

Complete contact information is available at: https://pubs.acs.org/10.1021/acs.jpcc.1c03630

Notes

The authors declare no competing financial interest.

■ ACKNOWLEDGMENTS

S.K. acknowledges ERC-2017-Starting Grant. This study received funding from the European Research Council (ERC) under the European Union's Horizon 2020 research and innovation program (ERC-2017-Starting Grant, grant agreement no. 756489-COSMOS).

■ REFERENCES

(1) Li, J.-R.; Sculley, J.; Zhou, H.-C. Metal-organic frameworks for separations. *Chem. Rev.* **2011**, *112*, 869−932.

(2) Kenarsari, S. D.; Yang, D.; Jiang, G.; Zhang, S.; Wang, J.; Russell, A. G.; Wei, Q.; Fan, M. Review of recent advances in carbon dioxide separation and capture. *RSC Adv.* **2013**, *3*, 22739−22773.

(3) Qiu, S.; Xue, M.; Zhu, G. Metal-organic framework membranes: from synthesis to separation application. *Chem. Soc. Rev.* **2014**, *43*, 6116−6140.

(4) Farha, O. K.; Eryazici, I.; Jeong, N. C.; Hauser, B. G.; Wilmer, C. E.; Sarjeant, A. A.; Snurr, R. Q.; Nguyen, S. T.; Yazaydın, A. Ö.; Hupp, J. T. Metal-Organic Framework Materials with Ultrahigh

Surface Areas: Is the Sky the Limit? *J. Am. Chem. Soc.* **2012**, *134*, 15016−15021.
(5) Yaghi, O. M.; O'Keeffe, M.; Ockwig, N. W.; Chae, H. K.; Eddaoudi, M.; Kim, J. Reticular synthesis and the design of new materials. *Nature* **2003**, *423*, 705−714.
(6) Keskin, S.; van Heest, T. M.; Sholl, D. S. Can metal-organic framework materials play a useful role in large-scale carbon dioxide separations? *ChemSusChem* **2010**, *3*, 879−891.
(7) Hu, Z.; Wang, Y.; Shah, B. B.; Zhao, D. CO_2 capture in metal−organic framework adsorbents: An engineering perspective. *Adv. Sustainable Syst.* **2019**, *3*, 1800080.
(8) Caskey, S. R.; Wong-Foy, A. G.; Matzger, A. J. Dramatic tuning of carbon dioxide uptake via metal substitution in a coordination polymer with cylindrical pores. *J. Am. Chem. Soc.* **2008**, *130*, 10870−10871.
(9) Wu, X.; Bao, Z.; Yuan, B.; Wang, J.; Sun, Y.; Luo, H.; Deng, S. Microwave synthesis and characterization of MOF-74 (M=Ni, Mg) for gas separation. *Microporous Mesoporous Mater.* **2013**, *180*, 114−122.
(10) Cohen, S. M. Postsynthetic methods for the functionalization of metal-organic frameworks. *Chem. Rev.* **2011**, *112*, 970−1000.
(11) Koutsianos, A.; Kazimierska, E.; Barron, A. R.; Taddei, M.; Andreoli, E. A new approach to enhancing the CO_2 capture performance of defective UiO-66 via post-synthetic defect exchange. *Dalton Trans.* **2019**, *48*, 3349−3359.
(12) Wu, Y.; Chen, H.; Xiao, J.; Liu, D.; Liu, Z.; Qian, Y.; Xi, H. Adsorptive separation of methanol-acetone on isostructural series of metal-organic frameworks M-BTC (M = Ti, Fe, Cu, Co, Ru, Mo): A computational study of adsorption mechanisms and metal-substitution impacts. *ACS Appl. Mater. Interfaces* **2015**, *7*, 26930−26940.
(13) Borycz, J.; Tiana, D.; Haldoupis, E.; Sung, J. C.; Farha, O. K.; Siepmann, J. I.; Gagliardi, L. CO_2 adsorption in M-IRMOF-10 (M = Mg, Ca, Fe, Cu, Zn, Ge, Sr, Cd, Sn, Ba). *J. Phys. Chem. C* **2016**, *120*, 12819−12830.
(14) Waitschat, S.; Fröhlich, D.; Reinsch, H.; Terraschke, H.; Lomachenko, K. A.; Lamberti, C.; Kummer, H.; Helling, T.; Baumgartner, M.; Henninger, S.; et al. Synthesis of M-UiO-66 (M = Zr, Ce or Hf) employing 2,5-pyridinedicarboxylic acid as a linker: defect chemistry, framework hydrophilisation and sorption properties. *Dalton Trans.* **2018**, *47*, 1062−1070.
(15) Feldblyum, J. I.; Liu, M.; Gidley, D. W.; Matzger, A. J. Reconciling the discrepancies between crystallographic porosity and guest access as exemplified by Zn-HKUST-1. *J. Am. Chem. Soc.* **2011**, *133*, 18257−18263.
(16) Garai, B.; Bon, V.; Krause, S.; Schwotzer, F.; Gerlach, M.; Senkovska, I.; Kaskel, S. Tunable flexibility and porosity of the metal-organic framework DUT-49 through postsynthetic metal exchange. *Chem. Mater.* **2020**, *32*, 889−896.
(17) Xue, W.; Wang, J.; Huang, H.; Mei, D. Structural and hydrolytic stability of coordinatively unsaturated metal-organic frameworks $M_3(BTC)_2$ (M = Cu, Co, Mn, Ni, And Zn): A combined DFT and experimental study. *J. Phys. Chem. C* **2021**, *125*, 5832−5847.
(18) Peedikakkal, A. M. P.; Aljundi, I. H. Mixed-metal Cu-BTC metal-organic frameworks as a strong adsorbent for molecular hydrogen at low temperatures. *ACS Omega* **2020**, *5*, 28493−28499.
(19) Sava Gallis, D. F.; Parkes, M. V.; Greathouse, J. A.; Zhang, X.; Nenoff, T. M. Enhanced O_2 selectivity versus N_2 by partial metal substitution in Cu-BTC. *Chem. Mater.* **2015**, *27*, 2018−2025.
(20) Mai, Z.; Liu, D. Synthesis and applications of isoreticular metal-organic frameworks IRMOFs-n (n = 1, 3, 6, 8). *Cryst. Growth Des.* **2019**, *19*, 7439−7462.
(21) Botas, J. A.; Calleja, G.; Sánchez-Sánchez, M.; Orcajo, M. G. Cobalt doping of the MOF-5 framework and its effect on gas-adsorption properties. *Langmuir* **2010**, *26*, 5300−5303.
(22) Zhou, Z.; Xing, X.; Tian, C.; Wei, W.; Li, D.; Hu, F.; Du, S. A multifunctional nanocage-based MOF with tri- and tetranuclear zinc cluster secondary building units. *Sci. Rep.* **2018**, *8*, 3117−3125.
(23) Yuan, J.; Liu, X.; Li, X.; Yu, J. Computer simulations for the adsorption and separation of $CH_4/H_2/CO_2/N_2$ gases by hybrid ultramicroporous materials. *Mater. Today Commun* **2021**, *26*, 101987.
(24) Avci, G.; Velioglu, S.; Keskin, S. In silico design of metal organic frameworks with enhanced CO_2 separation performances: Role of metal sites. *J. Phys. Chem. C* **2019**, *123*, 28255−28265.
(25) Lalonde, M.; Bury, W.; Karagiaridi, O.; Brown, Z.; Hupp, J. T.; Farha, O. K. Transmetalation: routes to metal exchange within metal-organic frameworks. *J. Mater. Chem. A* **2013**, *1*, 5453−5468.
(26) Altintas, C.; Erucar, I.; Keskin, S. High-throughput computational screening of the metal organic framework database for CH_4/H_2 separations. *ACS Appl. Mater. Interfaces* **2018**, *10*, 3668−3679.
(27) Moghadam, P. Z.; Li, A.; Liu, X.-W.; Bueno-Perez, R.; Wang, S.-D.; Wiggin, S. B.; Wood, P. A.; Fairen-Jimenez, D. Targeted classification of metal-organic frameworks in the Cambridge Structural Database (CSD). *Chem. Sci.* **2020**, *11*, 8373−8387.
(28) Allen, F. H. The Cambridge Structural Database: a quarter of a million cystal structures and rising. *Acta Crystallogr., Sect. B: Struct. Sci.* **2002**, *58*, 380−388.
(29) Avci, G.; Erucar, I.; Keskin, S. Do new MOFs perform better for CO_2 capture and H_2 purification? Computational screening of the updated MOF database. *ACS Appl. Mater. Interfaces* **2020**, *12*, 41567−41579.
(30) Bruno, I. J.; Cole, J. C.; Edgington, P. R.; Kessler, M.; Macrae, C. F.; McCabe, P.; Pearson, J.; Taylor, R. New software for searching the Cambridge Structural Database and visualizing crystal structures. *Acta Crystallogr., Sect. B: Struct. Sci.* **2002**, *58*, 389−397.
(31) Li, S.; Chung, Y. G.; Simon, C. M.; Snurr, R. Q. High-throughput computational screening of multivariate metal−organic frameworks (MTV-MOFs) for CO_2 capture. *J. Phys. Chem. Lett.* **2017**, *8*, 6135−6141.
(32) Qin, J.-S.; Yuan, S.; Wang, Q.; Alsalme, A.; Zhou, H.-C. Mixed-linker strategy for the construction of multifunctional metal-organic frameworks. *J. Mater. Chem. A* **2017**, *5*, 4280−4291.
(33) Wang, Y.; Feng, L.; Fan, W.; Wang, K.-Y.; Wang, X.; Wang, X.; Zhang, K.; Zhang, X.; Dai, F.; Sun, D.; et al. Topology exploration in highly connected rare-earth metal−organic frameworks via continuous hindrance control. *J. Am. Chem. Soc.* **2019**, *141*, 6967−6975.
(34) Erucar, I.; Keskin, S. High CO_2 selectivity of an amine-functionalized metal organic framework in adsorption-based and membrane-based gas separations. *Ind. Eng. Chem. Res.* **2013**, *52*, 3462−3472.
(35) Li, H.; Eddaoudi, M.; O'Keeffe, M.; Yaghi, O. M. Design and synthesis of an exceptionally stable and highly porous metal-organic framework. *Nature* **1999**, *402*, 276−279.
(36) Hafizovic, J.; Bjørgen, M.; Olsbye, U.; Dietzel, P. D. C.; Bordiga, S.; Prestipino, C.; Lamberti, C.; Lillerud, K. P. The inconsistency in adsorption properties and powder XRD data of MOF-5 is rationalized by framework interpenetration and the presence of organic and inorganic species in the nanocavities. *J. Am. Chem. Soc.* **2007**, *129*, 3612−3620.
(37) Lim, D.-W.; Chyun, S. A.; Suh, M. P. Hydrogen storage in a potassium-ion-bound metal-organic framework incorporating crown ether struts as specific cation binding sites. *Angew. Chem., Int. Ed.* **2014**, *53*, 7819−7822.
(38) Brozek, C. K.; Dincă, M. Lattice-imposed geometry in metal−organic frameworks: lacunary Zn_4O clusters in MOF-5 serve as tripodal chelating ligands for Ni^{2+}. *Chem. Sci.* **2012**, *3*, 2110−2113.
(39) Brozek, C. K.; Dincă, M. Ti^{3+}-, $V^{2+/3+}$-, $Cr^{2+/3+}$-, Mn^{2+}-, and Fe^{2+}-substituted MOF-5 and redox reactivity in Cr- and Fe-MOF-5. *J. Am. Chem. Soc.* **2013**, *135*, 12886−12891.
(40) Brozek, C. K.; Dincă, M. Thermodynamic parameters of cation exchange in MOF-5 and MFU-4l. *Chem. Commun.* **2015**, *51*, 11780−11782.
(41) Li, J.; Li, L.; Hou, H.; Fan, Y. Study on the reaction of polymeric zinc ferrocenyl carboxylate with Pb(II) or Cd(II). *Cryst. Growth Des.* **2009**, *9*, 4504−4513.

(42) Li, Y. L.; Liu, Y. S.; Yang, X. A new safety enrichment method for low concentration coal bed methane-proportion pressure swing adsorption. *Adv. Mat. Res.* **2011**, *233*−*235*, 2276−2280.
(43) Willems, T. F.; Rycroft, C. H.; Kazi, M.; Meza, J. C.; Haranczyk, M. Algorithms and tools for high-throughput geometry-based analysis of crystalline porous materials. *Microporous Mesoporous Mater.* **2012**, *149*, 134−141.
(44) Dubbeldam, D.; Calero, S.; Ellis, D. E.; Snurr, R. Q. RASPA: Molecular simulation software for adsorption and diffusion in flexible nanoporous materials. *Mol. Simul.* **2016**, *42*, 81−101.
(45) Rappé, A. K.; Casewit, C. J.; Colwell, K. S.; Goddard, W. A., III; Skiff, W. M. UFF, a full periodic table force field for molecular mechanics and molecular dynamics simulations. *J. Am. Chem. Soc.* **1992**, *114*, 10024−10035.
(46) Potoff, J. J.; Siepmann, J. I. Vapor-liquid equilibria of mixtures containing alkanes, carbon dioxide, and nitrogen. *AIChE J.* **2001**, *47*, 1676−1682.
(47) Buch, V. Path integral simulations of mixed para-D_2 and ortho-D_2 Clusters: The orientational effects. *J. Chem. Phys.* **1994**, *100*, 7610−7629.
(48) Martin, M. G.; Siepmann, J. I. Transferable potentials for phase equilibria. 1. United-atom description of n-alkanes. *J. Phys. Chem. B* **1998**, *102*, 2569−2577.
(49) Rappe, A. K.; Goddard, W. A. Charge equilibration for molecular dynamics simulations. *J. Phys. Chem.* **1991**, *95*, 3358−3363.
(50) Wilmer, C. E.; Snurr, R. Q. Towards rapid computational screening of metal-organic frameworks for carbon dioxide capture: Calculation of framework charges via charge equilibration. *Chem. Eng. J.* **2011**, *171*, 775−781.
(51) Lin, S.; Harada, M.; Suzuki, Y.; Hatano, H. Hydrogen production from coal by separating carbon dioxide during gasification. *Fuel* **2002**, *81*, 2079−2085.
(52) Bae, Y.-S.; Snurr, R. Q. Development and evaluation of porous materials for carbon dioxide separation and capture. *Angew. Chem., Int. Ed.* **2011**, *50*, 11586−11596.
(53) Li, Z.; Liu, P.; Ou, C.; Dong, X. Porous metal-organic frameworks for carbon dioxide adsorption and separation at low pressure. *ACS Sustainable Chem. Eng.* **2020**, *8*, 15378−15404.
(54) Han, S. S.; Jung, D.-H.; Heo, J. Interpenetration of metal organic frameworks for carbon dioxide capture and hydrogen purification: Good or bad? *J. Phys. Chem. C* **2013**, *117*, 71−77.
(55) Zhang, Z.; Yao, Z.-Z.; Xiang, S.; Chen, B. Perspective of microporous metal-organic frameworks for CO_2 capture and separation. *Energy Environ. Sci.* **2014**, *7*, 2868−2899.
(56) Sokhanvaran, V.; Yeganegi, S. Multiscale computational study on the adsorption and separation of CO_2/CH_4 and CO_2/H_2 on Li^+-doped mixed-ligand metal-organic framework $Zn_2(NDC)_2$(diPyNI). *ChemPhysChem* **2016**, *17*, 4124−4133.
(57) Daglar, H.; Keskin, S. Recent advances, opportunities, and challenges in high-throughput computational screening of MOFs for gas separations. *Coord. Chem. Rev.* **2020**, *422*, 213470.

https://doi.org/10.1021/acs.jpcc.1c03630
J. Phys. Chem. C 2021, 125, 17311−17322